2016 23rd International Conference on Pattern Recognition (ICPR)
Cancún Center, Cancún, México, December 4-8, 2016

Automatic cutting plane identification for computer-aided analysis of intracranial aneurysms

Tim Jerman, Franjo Pernuš, Boštjan Likar and Žiga Špiclin
Faculty of Electrical Engineering
University of Ljubljana
Tržaška 25, 1000 Ljubljana, Slovenia
Email: tim.jerman@fe.uni-lj.si

Aichi Chien
Division of Interventional Neuroradiology
Dept. of Radiology, UCLA Medical School
Los Angeles, California 90095
Email: aichi@ucla.edu

***Abstract*—Clinical studies have established the importance of morphologic measurements of intracranial aneurysm size, neck width, aspect ratio and other shape indices for the assessment of the risk of rupture and selection of the best treatment option. Obtaining these morphologic measurements requires segmentation of vascular structures in an angiographic image, reconstruction of a 3D vascular surface mesh, and isolation of the aneurysm surface mesh from parent vessels. High variability of aneurysm shapes appearing at various anatomical locations renders isolation of the aneurysm a critical step, which, if performed poorly, may adversely impact the morphologic measurements and possibly corrupt important information used for clinical assessment of the aneurysm. Previous quantitative validation of isolation methods showed that manual cutting plane based isolation is more accurate than isolation by state-of-the-art automatic methods. In this paper, we propose and quantitatively validate a novel method for automated cutting plane identification and aneurysm isolation based solely on analysis of the vascular surface mesh.**

I. Introduction

Intracranial aneurysms are a common cerebrovascular pathology, in which a weakened portion of cerebral arterial wall bulges to form a balloon-like structure that may eventually rupture and lead to subarachnoid hemorrhage, a serious health condition with a high mortality rate [1]. Several studies [2], [3], [4] established that morphologic measurements such as aneurysm size, neck width, aspect ratio and other shape indices [5], [6] are important factors for the assessment of risk of rupture and selection of the best treatment option, e.g. clipping or coiling. Because of their potentially high impact on treatment success and patient condition, the morphologic measurements of aneurysms must be obtained in an accurate and reliable manner.

Morphologic measurements are generally obtained by computer-aided analysis of angiographic images like digital subtraction angiography (DSA), and three–dimensional (3D) computed tomography angiography (CTA) or magnetic resonance angiography (MRA). To quantify an aneurysm, four major steps are required: 1) segmentation of the angiographic image which can be performed either by interactive manual segmentation or one of several automated methods [7] to extract vascular structures; 2) reconstruction of the vascular surface into a 3d mesh model; 3) isolation of the aneurysm surface mesh from the parent vessels and 4) computation of various size and shape indices based on the isolated aneurysm surface mesh.

High variability of aneurysm sizes and shapes, renders isolation of the aneurysm from parent vessels a very difficult task. The quality of the aneurysm isolation, however, has an immediate impact on the accuracy and reproducibility of morphologic measures. To isolate an aneurysm, its neck curve has to be delineated, which can be performed manually by interactive localization and interconnection of landmarks on the vessel surface [8]. Clearly, this is a tedious operation that is subject to high inter- and intra-operator variability.

In order to obtain neck curves that are accurate and reproducible several computer-aided methods [9], [10], [11], [12] were developed. Larrabide et al. [12] expanded a deformable tube model into parent vessels and then extracted the border between the tube model of parent vessel and the segmented vascular structures to obtain the neck curve. Mohamed et al. [10] employed a 3D deformable contour model to localize the aneurysm's neck and then isolate the aneurysm surface mesh. Cardenes et al. [11] and Ford et al. [9] computed a geodesic curve as the border between the aneurysm and the parent vessel using Voronoi regions on the surface mesh as a topologic restriction. These methods generally provide satisfactory neck curves for large (saccular) aneurysms that typically have a well defined neck, e.g. aneurysms whose inlet has considerably smaller cross-section than the aneurysm. However, if the cross-section of the aneurysm's inlet is similar or larger than the cross-section of the aneurysm, which is typical for small aneurysms, narrow elongated aneurysms, etc., these methods fail to adequately delineate the neck curve.

Cardenes et al. [8] compared the performance of two automatic aneurysm isolation methods, one using deformable model expansion [12] and the other geodesic curve computation with topological restrictions [11], and a simple isolation by manually positioning the cutting plane (MCP). The reference neck curve was obtained by interactive manual localization and interconnection of landmarks on the vessel surface [8]. Interestingly, quantitative validation of these methods on one synthetic and 26 real aneurysms showed that on average the MCP method performed better than the two automatic methods [8]. This is surprising in the sense that the MCP method assumes a planar neck curve, which generally is

978-1-5090-4846-5/16/$31.00 ©2016 IEEE

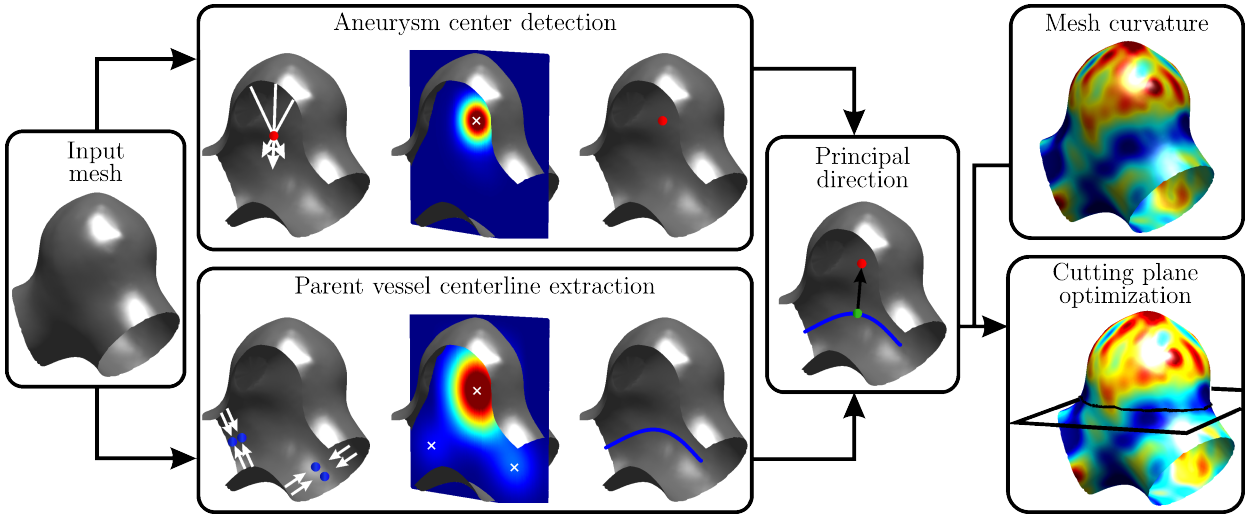

Fig. 1. Vascular surface mesh analysis framework for the detection of aneurysm center, parent vessel centerline extraction, aneurysm principal direction detection, and automatic cutting plane and neck curve extraction.

not the case. Nevertheless, based on these results a search for an optimal cross-section of a plane with the vascular surface mesh seems to be a promising approach to accurately and reliably identify a neck curve and by that isolate the aneurysm.

In this paper, we propose a novel method for automated cutting plane (ACP) identification based on the analysis of a vascular surface mesh. The method first detects the aneurysm center and parent vessel centerlines by analyzing surface normals. This information is than used to compute a direction vector from the parent vessel centerline through the center of aneurysm. The obtained direction serves as a normal of the initial cutting plane, which is then refined by maximizing the integral of Gaussian curvature of the vascular surface mesh along a cross-section of the cutting plane and the mesh. The proposed method was evaluated and compared to the MCP identified by a clinician on five datasets of intracranial aneurysms. The comparison of curve-based and morphologic measurements showed a very good agreement between the ACP and MCP methods.

II. Method

Automatic detection of the aneurysm's cutting plane is performed on a triangulated surface mesh $\mathcal{M}$ of the aneurysm and its parent vessels. Given an input 3D angiographic image, the aneurysm was first detected using a Hessian based filter that enhances spherical structures [13], then the vascular structures in a local rectangular region surrounding the aneurysm were segmented [7]. The resulting 3D volume contained the segmentation of a whole aneurysm together with all its parent vessels in a local neighborhood, and was used to create a 3D surface mesh. The surface mesh is the input to the method for isolation of an aneurysm based on automatic identification of a cutting plane, which is performed in four steps:

A. Detection of the aneurysm center based on the analysis of surface normals.
B. Detection of the parent vessel centerline based on the analysis of surface normals.
C. Estimation of the direction vector from a point on the detected parent vessel centerline through the center of aneurysm.
D. Cutting plane identification by maximization of the integral of Gaussian curvature computed for each vertex on the surface mesh $\mathcal{M}$.

Overview of the main steps of the method is shown in Fig. 1.

A. Detection of aneurysm center

Aneurysm center is an important reference point that can be used to determine the principal direction from the parent vessel centerline through the aneurysm center. This direction vector is an important reference when the cutting plane is manually positioned and is generally a good estimate of the cutting plane's normal. Consequently, the position of the aneurysm's center has to be accurately detected.

Development of the center point detection method was based on the assumption that partial surface patches of the aneurysm are approximately spherical. Therefore, the center point can be detected as an intersection point $\mathbf{x} = (x, y, z)$ of three vectors $\mathbf{v}_i$, $i = 1, 2, 3$, which originate on the triangulated mesh surface and point in the direction opposite to the surface normals $\mathbf{n}_\mathcal{M}$: $\mathbf{v}_i = -\mathbf{n}_\mathcal{M}$. For a robust estimation of the aneurysm center, we performed an exhaustive random sampling of N_T triplets that resulted in several candidate center points $\mathcal{C} = \mathbf{x}_c; c = 1 \dots N_T$. To suppress possible outliers, a candidate center $\mathbf{x}_c$ is rejected when the shortest distance from each $\mathbf{v}_i^c$ to their estimated intersection is larger than some threshold value T_d. The obtained candidate center points and the corresponding distances $d_{c,\mathcal{M}}$ to the nearest vertex on the surface mesh are used to build an accumulator image. The accumulator image A_A is a 3D rasterized image with the size corresponding to the local rectangular region surrounding the aneurysm. All values in the accumulator

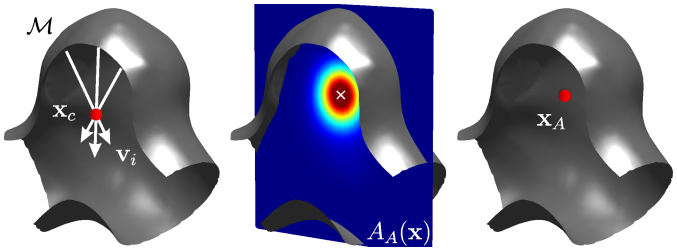

Fig. 2. Aneurysm center point detection based on accumulating the intersection locations of surface normal triplets. The highest response in the accumulator corresponds to the aneurysm center.

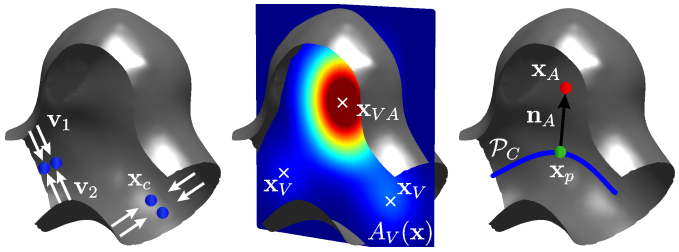

Fig. 3. Detection of parent vessel centerlines (*blue line*) and the locations of inlet points based on accumulating the halfway locations between surface location with anticollinear normals. This information is used to determined the principal direction (*black arrow*) originating at the centerline (*green point*) through the aneurysm center (*red point*).

image are initially set to zero. Then, for each candidate center point $\mathbf{x}_c \in \mathcal{C}$, a 3D Gaussian $\mathcal{G}(\mathbf{x}_c; \sigma)$ centered at $\mathbf{x}_c$ with a standard deviation equal to $\sigma = d_{c,\mathcal{M}}/2$ is added to the accumulator A_A:

$$A_A(\mathbf{x}) = A_A(\mathbf{x}) + \mathcal{G}(\mathbf{x}_c - \mathbf{x}; d_{c,\mathcal{M}}/2) \quad (1)$$

After accumulation is performed for all candidate points, the location of maximal value in the accumulator $\mathbf{x}_A = \text{argmax}_{\mathbf{x}}\, A_A(\mathbf{x})$ is determined as the aneurysm's center point. The main steps of the center point detection method are shown in Figure 2.

B. Detection of parent vessel centerline

Vessel centerline is generally defined as the center of the vessel's cross-section, which is close to circular. However, in the vicinity of an aneurysm there are large morphologic deviations like irregular swelling of the vessel, which make the automatic detection of the centerline very difficult. To address this problem, we propose to first detect the centerlines of the parent vessel inlets, which are further away from the aneurysm and thus their shape is less affected by the presence of an aneurysm. These centerlines serve as two anchor points between which the shortest line through the aneurysm is determined using the fast marching algorithm [14].

Centerlines of the parent vessel inlets are found by an approach similar to the aneurysm center detection method. For each vertex $\mathbf{x}_{v1}$ in the mesh $\mathcal{M}$, a ray is casted in the direction opposite to the surface normal $\mathbf{v}_1 = -\mathbf{n}_{\mathcal{M}}(\mathbf{x}_{v1})$. If the ray intersects the surface mesh, then the closest vertex $\mathbf{x}_{v2}$ and its corresponding normal $\mathbf{v}_2 = -\mathbf{n}_{\mathcal{M}}(\mathbf{x}_{v2})$ are determined. A candidate vessel center point $\mathbf{x}_c$ is found halfway between $\mathbf{x}_{v1}$ and $\mathbf{x}_{v2}$ and the point $\mathbf{x}_c$ is retained only if vectors $\mathbf{v}_1$ and $\mathbf{v}_2$ are approximately anticollinear ($\mathbf{v}_1 \approx -\mathbf{v}_2$). This condition is valid for vessels with circular or even elliptic cross-sections. Using a collection of N_C candidate points $\mathcal{C} = \mathbf{x}_c; c = 1 \ldots N_C$, an accumulator image $A_V(\mathcal{C})$ is initialized to zero and update similar as in (1). Searching for local maxima in the obtained accumulator yields the locations of the inlet centers of the parent vessel $\mathbf{x}_V$ and of the aneurysm center $\mathbf{x}_{VA}$ (Figure 3). The obtained aneurysm center $\mathbf{x}_{VA}$ is not well localized compared to the previously detected aneurysm center point $\mathbf{x}_A$ (Sec. II-A). Therefore, the location $\mathbf{x}_{VA}$ is a priori rejected by having the minimal distance to the previously extracted aneurysm center point $\mathbf{x}_A$, whereas the remaining vessel inlet centers are used to retrieve the centerline of the parent vessel.

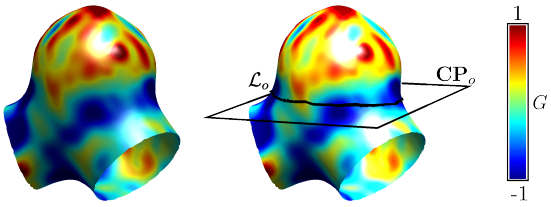

Fig. 4. The color-coded values of the Gaussian curvature G computed on the vascular surface mesh are used to obtain the optimal cutting plane CP and the corresponding neck curve (*black line*) is defined as the cross-section between the mesh and CP.

Using the fast marching algorithm [14] a distance map is computed between the detected inlet points $\mathbf{x}_V$, and a connecting path $\mathcal{P}$ with the shortest distance $|\mathcal{P}|$ determining the vessel centerline $\mathcal{P}_C$. To constrain the shortest path to lie near the expected vessel centerline, the computation of the distance maps is weighted with the values of accumulator A_V, in which higher values lie near the vessel centerline.

C. Initial cutting plane normal

The computed centerline $\mathcal{P}_C$ and aneurysm center point $\mathbf{x}_A$ are used to determine the principal direction $\mathbf{n}_A$ of the aneurysm's dome. The direction $\mathbf{n}_A$ is defined as a vector from $\mathcal{P}_C(\mathbf{x_p})$ to $\mathbf{x}_A$, where $\mathbf{x}_p$ is a point on the centerline, determined by minimizing the length of $|\mathbf{n}_A|$. The obtained direction is used as a normal of the initial cutting plane.

D. Cutting plane identification

Because an aneurysm is a local dilation of the vessel and the neck curve should separate the aneurysm from its parent vessel there should be a change in the measured Gaussian surface curvature near a tentative aneurysm neck. The curvature change is especially prominent in larger saccular aneurysms, but can also be observed in smaller aneurysms. The values of the Gaussian curvature G [15] computed on the mesh are generally lower in the neck region compared to the other parts of the aneurysm (Figure 4, *left*).

A cutting plane $\mathbf{CP}$ has a corresponding neck curve $\mathcal{L}$, which is defined as the intersection between $\mathbf{CP}$ and $\mathcal{M}$.

TABLE I

QUANTITATIVE COMPARISON BETWEEN MANUAL AND AUTOMATIC ANEURYSM'S NECK CURVE DELINEATION USING THREE CLINICAL MEASURES: AVERAGE NECK WIDTH (NW), DOME HEIGHT (DH), AND ASPECT RATIO (AR). THE CASE SEQUENCE EQUALS TO THE ONE ON FIG. 5.

Metric	Case 1		Case 2		Case 3		Case 4		Case 5	
	Manual	Autom.	Manual	Autom.	Manual	Autom.	Manual	Autom.	Manual	Autom.
NW [mm]	7.23	7.15	3.88	3.95	4.06	4.07	4.09	4.18	3.00	2.95
DH [mm]	5.10	4.96	3.41	3.56	3.18	3.20	3.52	3.67	3.53	3.60
AR	1.42	1.44	1.14	1.11	1.28	1.27	1.16	1.14	0.85	0.82

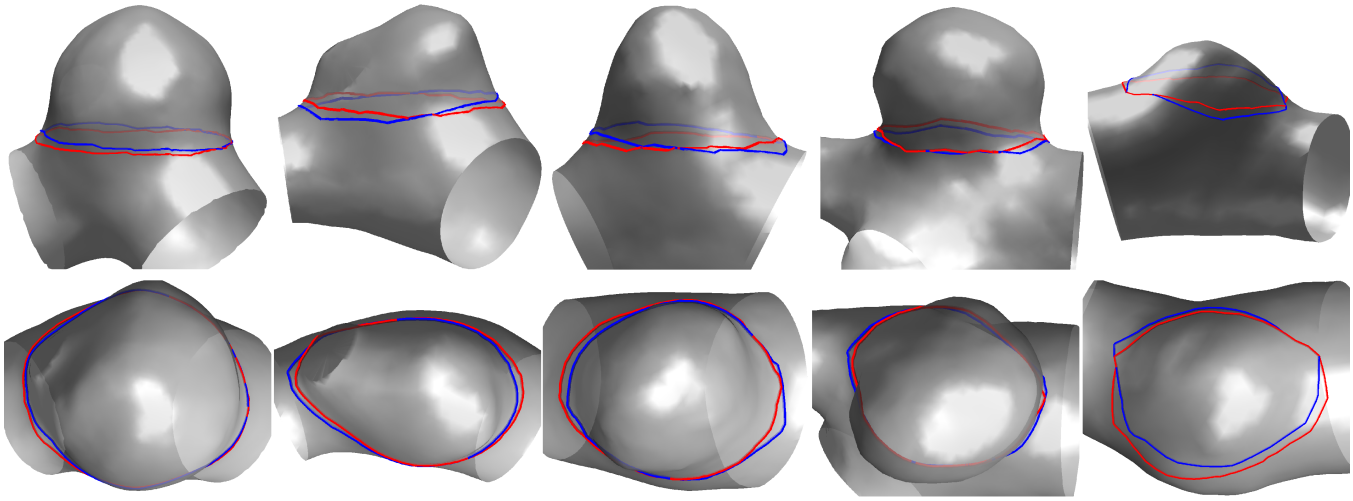

Fig. 5. Two views of the aneurysm neck curve obtained by manually (*red*) and automatically (*blue*) defined cutting plane for five intracranial aneurysms (*from left to right*: Case 1–5).

An optimization method identifies a cutting plane such that the integral of G over the closed curve $\mathcal{L}$ defined by CP is minimized:

$$\mathcal{L}^* = \underset{\mathcal{L} \subset CP}{\operatorname{argmin}} \oint_{\mathcal{L}} G(x)dx \tag{2}$$

The locations z along the initial cutting plane normal $\mathbf{n}_A$ between the point on the parent vessel centerline and the aneurysm center are used as the possible origins of the plane, while orientation (θ_{CP}, ϕ_{CP}) in spherical coordinates that corresponds to the initial cutting plane normal $\mathbf{n}_{CP}$ is also refined. The optimal cutting plane $\mathbf{CP}_o$ is found by an exhaustive search over its (θ, ϕ, z) parameters, where θ and ϕ define the rotation angle with respect to θ_{CP} and ϕ_{CP} and z defines the height of the normal's origin in the direction of $\mathbf{n}_{CP}$. The cross-section of the optimized cutting plane $\mathbf{CP}_o$ with the vascular surface mesh $\mathcal{M}$ yields an optimized neck curve $\mathcal{L}_o$ (Figure 4, *right*).

III. EXPERIMENTS AND RESULTS

The proposed method for automatic cutting plane identification and neck curve extraction was evaluated on a dataset of five intracranial aneurysms. For each of the aneurysms a reference neck curve was created using a manual cutting plane (i.e. the MCP method), which was positioned by a trained neuroradiologist. Aneurysm neck curves were determined for both the proposed ACP and MCP methods, the aneurysm was isolated and several morphologic measures were computed and cross-compared. Since the MCP represents a reference cutting plane, the morphologic measures obtained with the use of ACP should be as similar as possible to those obtained with MCP. Furthermore, the neck curves obtained by the proposed ACP and MCP methods were also directly compared.

Three morphologic measures were computed: 1) average neck width (NW), 2) dome height (DH), and 3) aspect ratio (AR). The NW is defined as the average of the distances of connecting lines between all pairs of points that lie opposite to each other on the neck curve. The intersection of these lines represented the center of the neck curve. Distance between the neck curve center and furthest point inside the aneurysm was used as a measure of the DH. The AR was computed as a ratio between NW and DH, and is one of the most important measures used to determine the risk of rupture of an aneurysm [6]. Table I presents the NW, DH, and AR values obtained for five aneurysms from the manually and automatically extracted neck curves, based on MCP and ACP, respectively. The difference between the automatic and reference manual neck curves was consistently small with respect to all three metrics and independent of the size or shape of the aneurysm, which is very important for a clinical applications of such methods.

For curve-based evaluation the average symmetric curve distance (ASCD) between the automatic and reference manual neck curves was computed. The ASCD was defined as the average of the distances between all pairs of corresponding

TABLE II
AVERAGE SYMMETRIC CURVE DISTANCE (ASCD), IN MILLIMETERS AND IN PERCENTAGE OF THE DOME HEIGHT (DH), BETWEEN MANUAL AND AUTOMATIC ANEURYSM'S NECK CURVE DELINEATIONS.

Metric	Case 1	Case 2	Case 3	Case 4	Case 5
ASCD [mm]	0.22	0.13	0.17	0.15	0.14
ASCD [% DH]	4.23	3.87	5.25	4.37	4.05

(closest) points on the ACP and MCP curves. The values of computed ASCD between the five pairs of curves are summarized in Table II. On average the ASCD was lower than 0.2 millimeters and represented approximately 4% of the aneurysms' DH.

A qualitative comparison of the extracted neck curves is shown in Fig. 5, where all five aneurysms and the corresponding manual and automatic neck curves are overlayed on the vascular surface mesh. Visual comparison of the curves confirms the small differences between the ACP and MCP as obtained in the curve-based evaluation (Table II). The results indicate that the proposed automatic method successfully simulates the manual placement of the cutting plane. Moreover, for the smallest aneurysm where the neck is poorly defined (Fig. 5, *right*) and where other more complex automated methods generally fail, the cutting plane was correctly determined by the proposed ACP method.

IV. DISCUSSION

Studies showed that the risk of rupture of an aneurysm can be assessed by quantitative measures of the aneurysm's morphology [6], [16]. Since the chance of aneurysm rupture is generally low, each detected aneurysm is carefully assessed so as to determine the optimal treatment option. In general, only those aneurysms with a high probability of rupture are treated because the risk of rupture outweighs the risk of complications during the treatment [4]. One of the most important metrics in determining the risk of rupture is aspect ratio, computed as the ratio between dome height and average neck diameter. Aneurysms that have a higher predictive chance of rupture have a higher value of the aspect ratio [6], [16]. Hence, accurate and reliable morphologic measurement of the aneurysms from angiographic images is important for their assessment, monitoring and to select the best treatment at the best moment.

Aneurysm assessment requires segmentation of the angiographic image in order to extract the vascular structures, followed by reconstruction of a 3D vascular surface mesh, isolation of the aneurysm surface mesh from parent vessels and, finally, computation of the morphologic measures. High variability of aneurysms' shape and anatomical location make the process of isolation a critical step, which, if performed poorly, may adversely impact the morphologic measurements and possibly corrupt important information used for clinical assessment of the aneurysm.

Cardenes et al. [8] compared the performance of two automatic isolation methods and a manual method based on positioning the cutting plane (i.e. the MCP) and found that the MCP method generally performs better than the two automatic methods. For instance, the MCP had the lowest average inter curve distance with respect to a manually outlined neck curve used as reference. In order to minimize possibly high inter- and intra-operator variability that may result from manual placement required with the MCP, we devised a novel method that automatically identifies the cutting plane (i.e. the ACP) and the corresponding neck curve to isolate the aneurysm.

The quantitative evaluation in Table I showed a highly comparable morphological measures like NW, DH and AH between the ACP and MCP based neck curves computed across five intracranial aneurysms. The relative error observed for the three measures was low, ranging from -1.67% to 2.20%, -3.75% to 4.40% and -3.53% to 1.41% for NW, DH and AR, respectively. The averaged absolute values of the relative error are all below 2.80%, which is almost twice lower compared to values on clinical datasets reported by Cardenes et al. [8]. A similar improvement was obtained with the ASCD metric where the proposed method achieved a mean distance between curves of 0.16 mm, which is significantly lower compared to the reported values of 0.5 mm from Cardenes et al.

Although the isolation based on a cutting plane is simple and effective, its main limitation is the assumption that the neck curve is planar, which obviously is not always the case. Due to this assumption it is often difficult to determine a cutting plane such that would not skip minor sections of dilated vessel near the aneurysm, which might potentially impact the morphologic measurements. In order to alleviate measurement errors in such situations, the extraction of the aneurysm's neck curve based on the automatic positioning of the cutting plane could be further improved by further refining the neck curve independently of the cutting plane based on geodesic distance and Gaussian curvature as the guiding criteria. We expect that neck curves obtained in this way would better capture the dilated parts of the vessel. Such methodological improvements to the neck curve extraction will be the aim of our future work as they could give an edge over the cutting plane based neck curve extraction and lead to more accurate morphologic aneurysm quantification.

V. CONCLUSION

We proposed novel methods for detecting the aneurysm center and the centerline of parent vessels based solely on the vascular surface mesh analysis. These methods were jointly employed in a novel method for automatic cutting plane identification for the purpose of aneurysm isolation. Quantitative and visual evaluations of the proposed method on a dataset of five differently shaped and sized intracranial aneurysms showed a high agreement between the morphologic measurements and small inter curve distances obtained either by automatically or manually determined cutting planes. The consistency observed in the clinically established morphologic measures NW, DH, and AR shows the potential for future clinical use of the proposed method.

ACKNOWLEDGMENT

This research was supported by the Slovenian Research Agency under grants J2-7118, J2-7211, J2-5473, L2-5472, and J7-6781, and in part, by the Brain Aneurysm Foundation, Timothy P. Susco Chair of Research, Research Grant, and by a UCLA Radiology Exploratory Research Grant. Authors are grateful to Vicki Lau for assistance with data collection.

REFERENCES

[1] J. L. Brisman, J. K. Song, and D. W. Newell, "Cerebral aneurysms," *New Engl. J. Med.*, vol. 355, no. 9, pp. 928–939, Aug. 2006.

[2] M. Sonobe, T. Yamazaki, M. Yonekura, and H. Kikuchi, "Small Unruptured Intracranial Aneurysm Verification Study SUAVe Study, Japan," *Stroke*, vol. 41, no. 9, pp. 1969–1977, Sep. 2010.

[3] J. P. Villablanca, G. R. Duckwiler, R. Jahan, S. Tateshima, N. A. Martin, J. Frazee, N. R. Gonzalez, J. Sayre, and F. V. Vinuela, "Natural History of Asymptomatic Unruptured Cerebral Aneurysms Evaluated at CT Angiography: Growth and Rupture Incidence and Correlation with Epidemiologic Risk Factors," *Radiology*, vol. 269, no. 1, pp. 258–265, Oct. 2013.

[4] R. D. Brown Jr and J. P. Broderick, "Unruptured intracranial aneurysms: epidemiology, natural history, management options, and familial screening," *The Lancet Neurology*, vol. 13, no. 4, pp. 393–404, Apr. 2014.

[5] B. Ma, R. E. Harbaugh, and M. L. Raghavan, "Three-Dimensional Geometrical Characterization of Cerebral Aneurysms," *Annals of Biomedical Engineering*, vol. 32, no. 2, pp. 264–273, Feb. 2004.

[6] S. Dhar, M. Tremmel, J. Mocco, M. Kim, J. Yamamoto, A. H. Siddiqui, L. N. Hopkins, and H. Meng, "Morphology Parameters for Intracranial Aneurysm Rupture Risk Assessment," *Neurosurgery*, vol. 63, no. 2, pp. 185–197, Aug. 2008.

[7] D. Lesage, E. D. Angelini, I. Bloch, and G. Funka-Lea, "A review of 3d vessel lumen segmentation techniques: Models, features and extraction schemes," *Med. Image Anal.*, vol. 13, no. 6, Dec. 2009.

[8] R. Cardenes, I. Larrabide, L. S. Romn, and A. F. Frangi, "Performance assessment of isolation methods for geometrical cerebral aneurysm analysis," *Medical & Biological Engineering & Computing*, vol. 51, no. 3, pp. 343–352, Mar. 2013.

[9] M. D. Ford, Y. Hoi, M. Piccinelli, L. Antiga, and D. A. Steinman, "An objective approach to digital removal of saccular aneurysms: technique and applications," *The British Journal of Radiology*, vol. 82, no. special_issue_1, pp. S55–S61, Jan. 2009.

[10] A. Mohamed, E. Sgouritsa, H. Morsi, H. Shaltoni, M. E. Mawad, and I. A. Kakadiaris, "Computer-aided planning for endovascular treatment of intracranial aneurysms (CAPETA)," in *SPIE, Medical Imaging 2010: Visualization, Image-Guided Procedures, and Modeling*, K. H. Wong and M. I. Miga, Eds., 2010, pp. 762 532–9.

[11] R. Cardenes, J. Pozo, H. Bogunovic, I. Larrabide, and A. Frangi, "Automatic Aneurysm Neck Detection Using Surface Voronoi Diagrams," *IEEE Transactions on Medical Imaging*, vol. 30, no. 10, pp. 1863–1876, Oct. 2011.

[12] I. Larrabide, M. C. Villa-Uriol, R. Crdenes, J. M. Pozo, J. Macho, L. S. Roman, J. Blasco, E. Vivas, A. Marzo, D. R. Hose, and A. F. Frangi, "Three-dimensional morphological analysis of intracranial aneurysms: A fully automated method for aneurysm sac isolation and quantification," *Medical Physics*, vol. 38, no. 5, pp. 2439–2449, May 2011.

[13] T. Jerman, F. Pernus, B. Likar, and Z. Spiclin, "Blob enhancement and visualization for improved intracranial aneurysm detection," *IEEE Transactions on Visualization and Computer Graphics*, no. 99, pp. 1–1, 2015.

[14] "Fast extraction of minimal paths in 3d images and applications to virtual endoscopy1," *Medical Image Analysis*, vol. 5, no. 4, pp. 281 – 299, 2001.

[15] B. Hamann, *Geometric Modelling*. Springer Vienna, 1993, ch. Curvature Approximation for Triangulated Surfaces.

[16] M. L. Raghavan, B. Ma, and R. E. Harbaugh, "Quantified aneurysm shape and rupture risk," *Journal of Neurosurgery*, vol. 102, no. 2, pp. 355–362, Feb. 2005.